

## Supporting information

### **The release of metal ions induced surface reconstruction of layered double hydroxide electrocatalyst**

Yu-Xun Zhu <sup>a</sup>, Min Liu <sup>b</sup>, Guang-Ya Hou <sup>a</sup>, Yi-Ping Tang <sup>a, \*</sup>, Lian-Kui Wu <sup>a, c, \*</sup>

a. College of Materials Science and Engineering, Zhejiang University of Technology,

Hangzhou 310014, China

b. State Grid Zhejiang Electric Power CO., LTD. Research Institute, Hangzhou 310014, China

c. School of Materials, Sun Yat-sen University, Shenzhen 518107, China

E-mail: [tangyiping@zjut.edu.cn](mailto:tangyiping@zjut.edu.cn) (Yi-Ping Tang) [wulk5@mail.sysu.edu.cn](mailto:wulk5@mail.sysu.edu.cn) (Lian-Kui Wu)

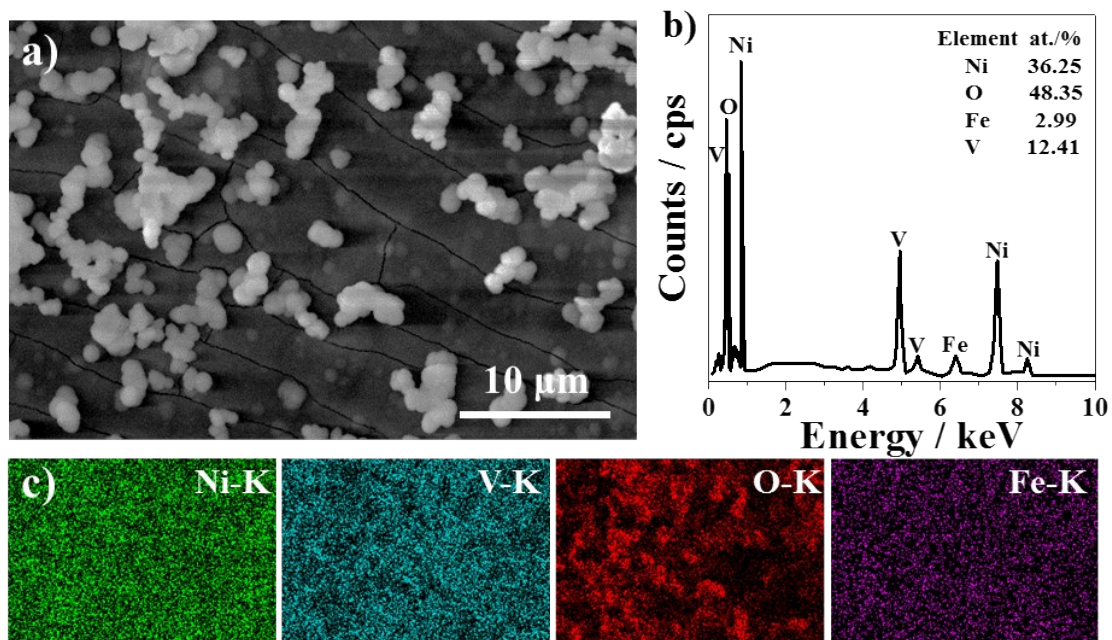


**Figure S1.** SEM image (a), EDS pattern (b), and corresponding elemental mapping images (c) of O-NiFeV-LDH.

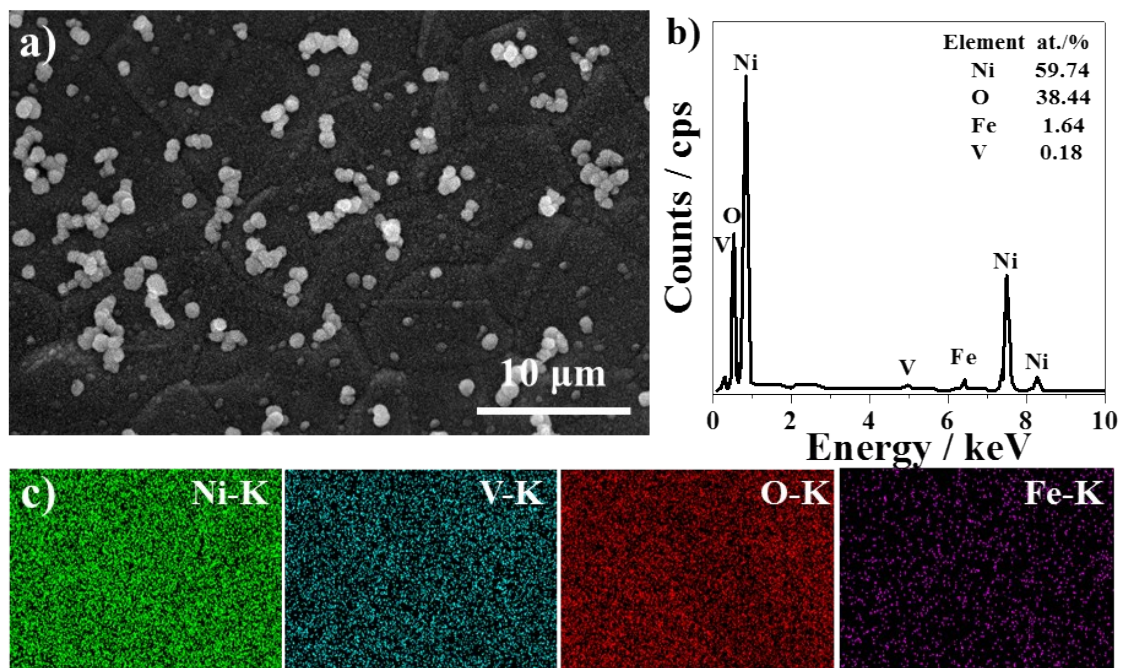


**Figure S2.** SEM image (a), EDS pattern (b), and corresponding elemental mapping images (c) of A-NiFeV-LDH.

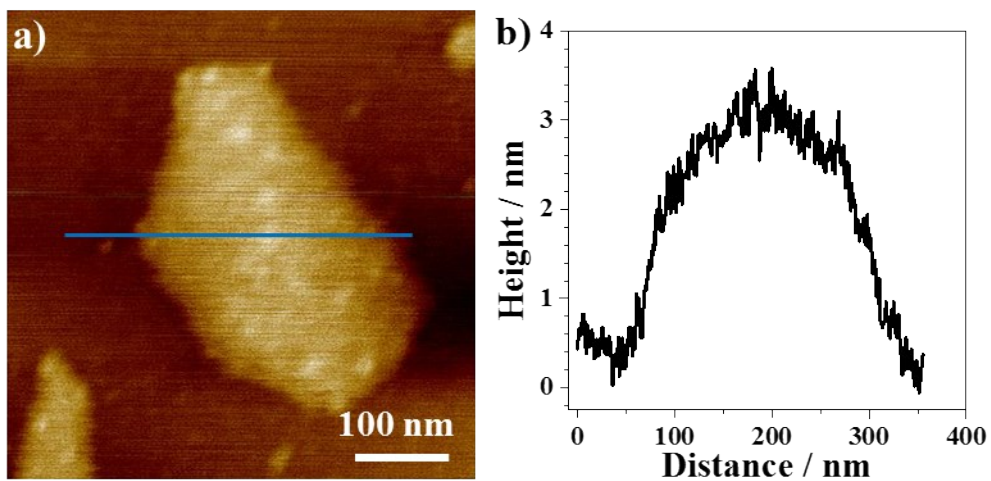


**Figure S3.** Representative AFM image (a) and corresponding line scan profile (b) of one O-NiFeV-LDH sheet deposited on a mica substrate.

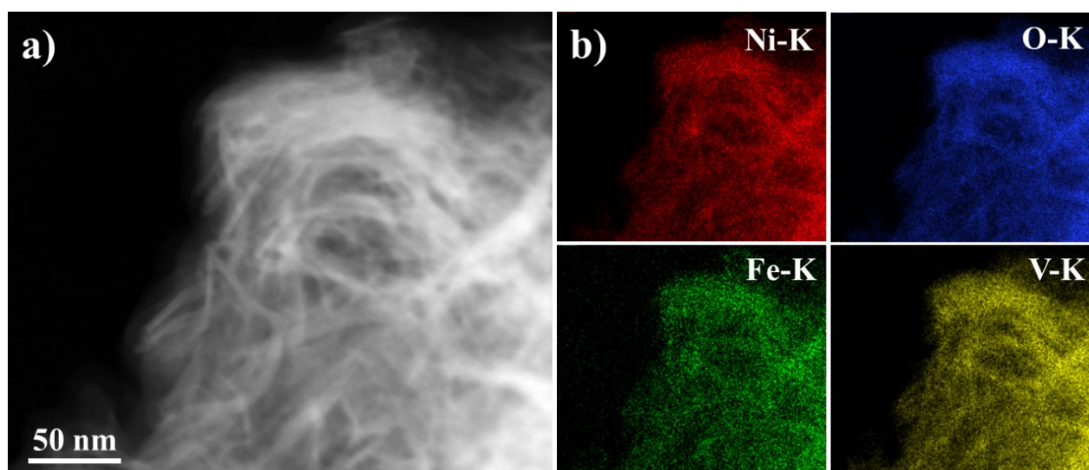


**Figure S4.** HAADF image (a) and corresponding STEM-EDS elemental mapping (Ni, O, Fe, and V) (b) of O-NiFeV-LDH.

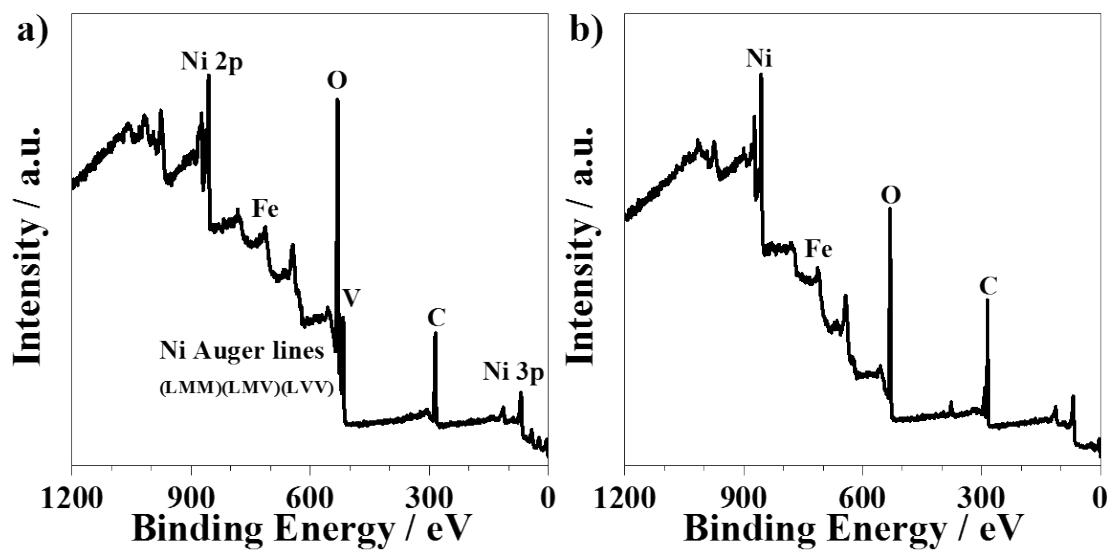


**Figure S5.** Survey XPS spectra of O-NiFeV-LDH (a) and A-NiFeV-LDH (b).

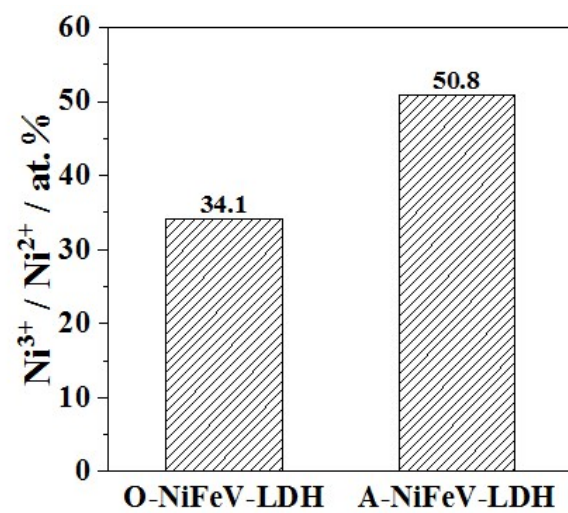


**Figure S6.** The valence state ratio of nickel ( $\text{Ni}^{3+} / \text{Ni}^{2+}$ ) of O-NiFeV-LDH and A-NiFeV-LDH.

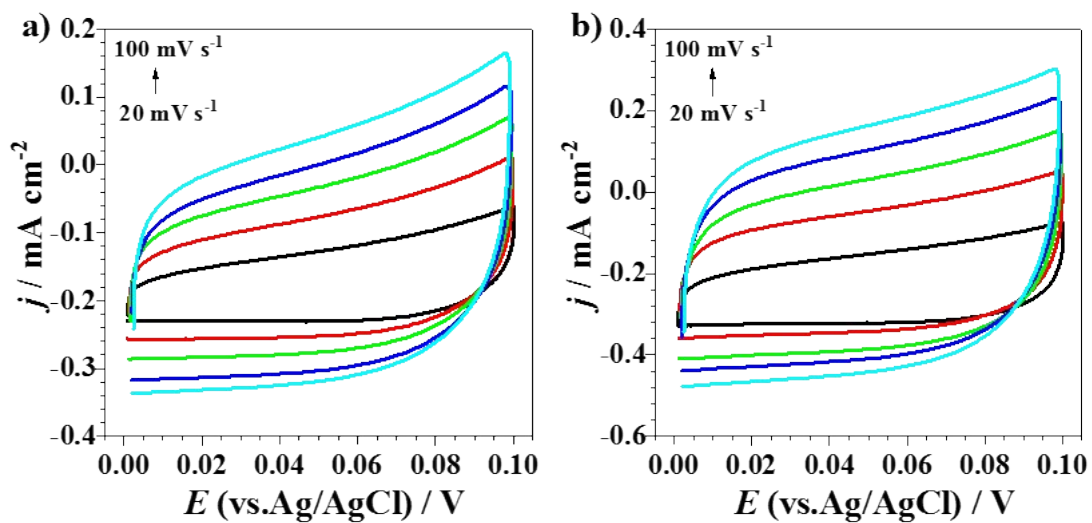


**Figure S7.** CV curves in the double layer region with various scan rates from 20 to 100  $\text{mV s}^{-1}$  for O-NiFeV-LDH (a) and A-NiFeV-LDH (b).



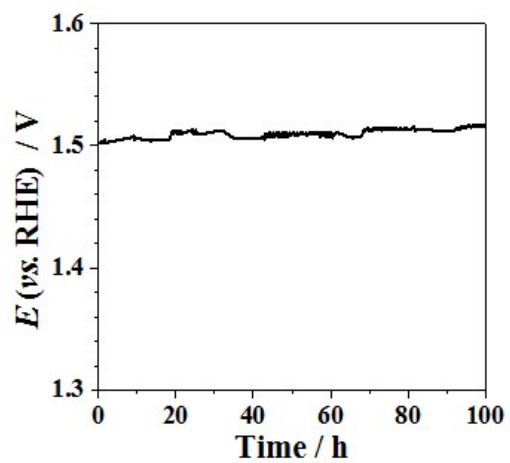


**Figure S8.** Chronopotentiometry curves of A-NiFeV-LDH during electrolysis at constant current densities of  $10 \text{ mA cm}^{-2}$  in  $1.0 \text{ M KOH}$ .

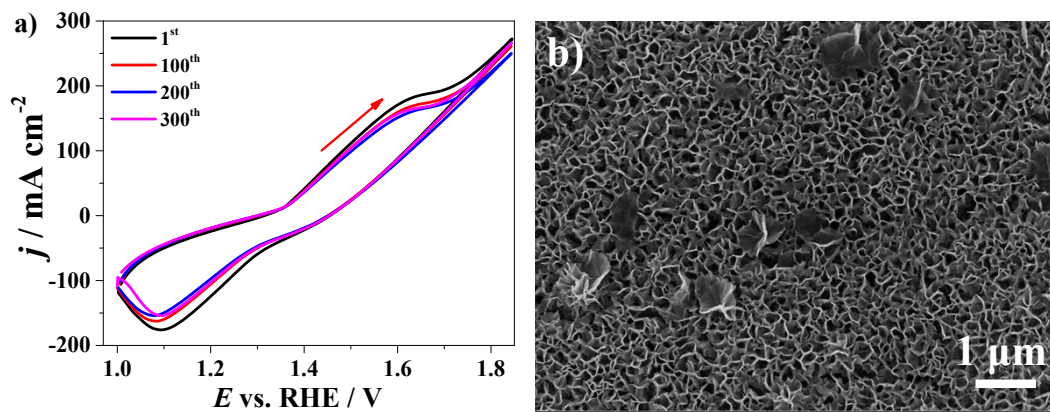


**Figure S9.** (a) 1<sup>st</sup> - 300<sup>th</sup> CV curves of A-NiFeV-LDH at a scan rate of 50  $\text{mV s}^{-1}$  in 1.0 M KOH. (b) SEM image of A-NiFeV-LDH after 300 consecutive CV scans.

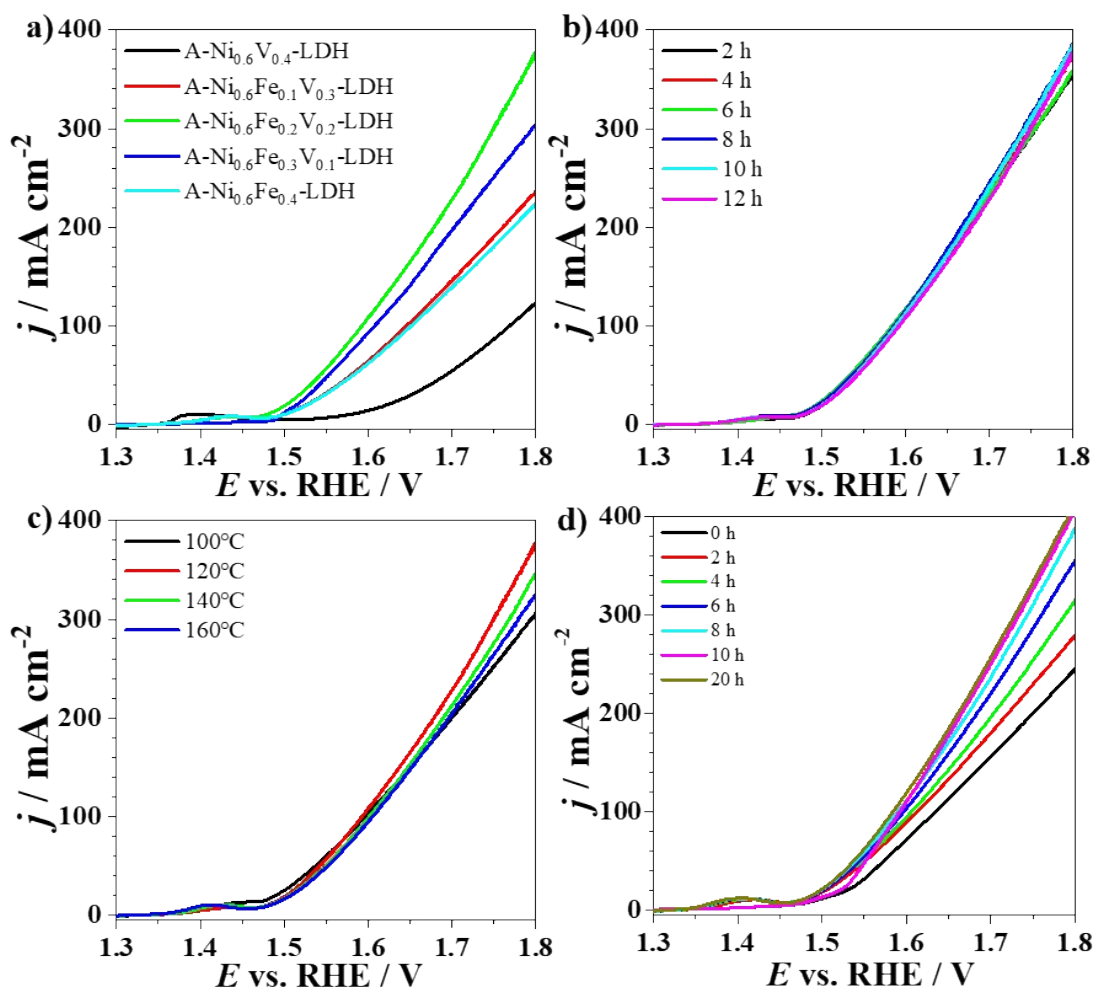


**Figure S10.** The influence of  $\text{Fe}^{3+}$  and  $\text{V}^{3+}$  concentrations (a), hydrothermal time (b), hydrothermal temperature (c), and activation time (d) on the LSV performance of A-NiFeV-LDH.

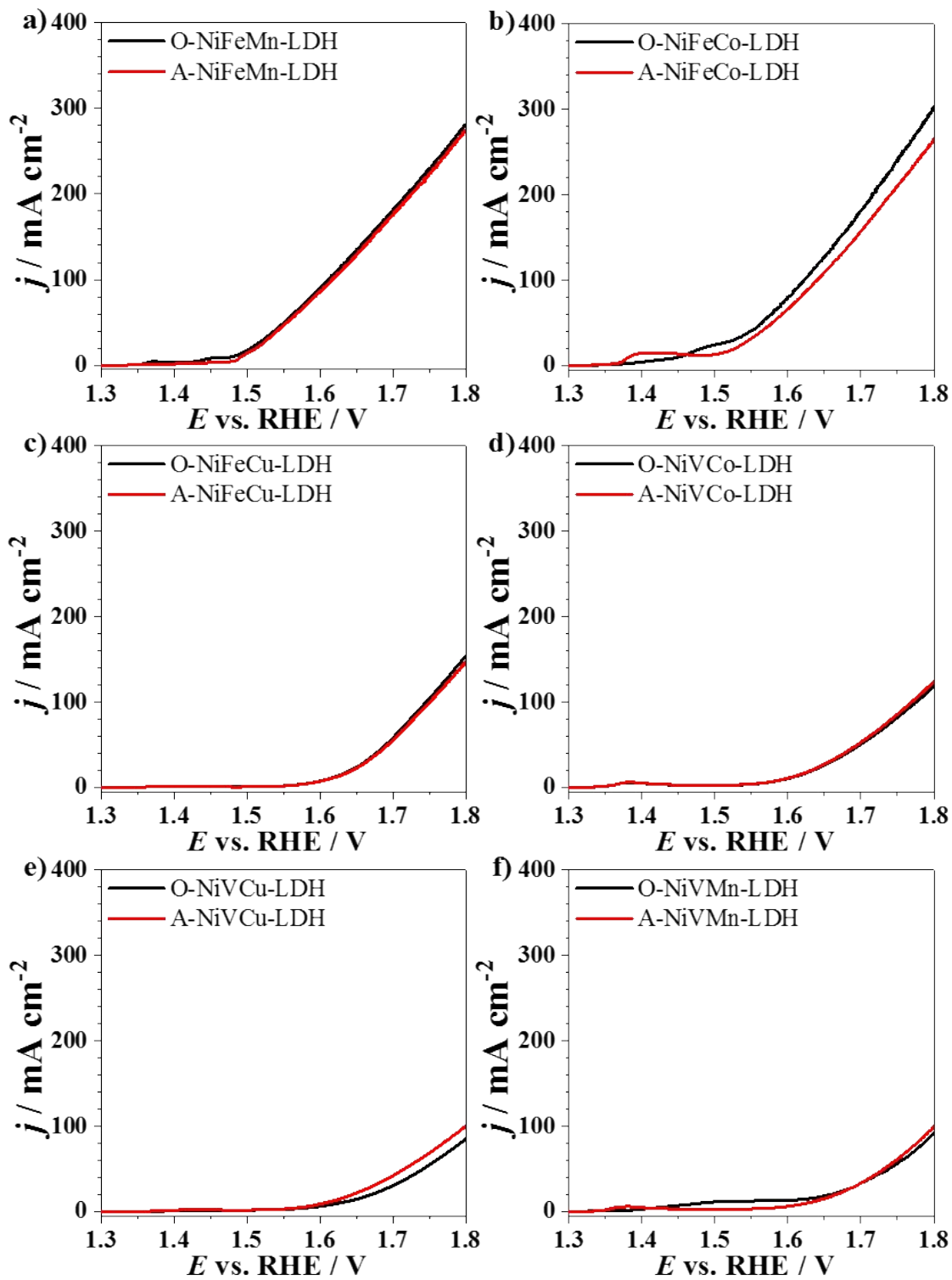


**Figure S11.** LSV curves of Ni-based LDHs before and after activation for 10 h: NiFeMn (a), NiFeCo (b), NiFeCu (c), NiVCo (d), NiVCu (e), and NiVMn (f).

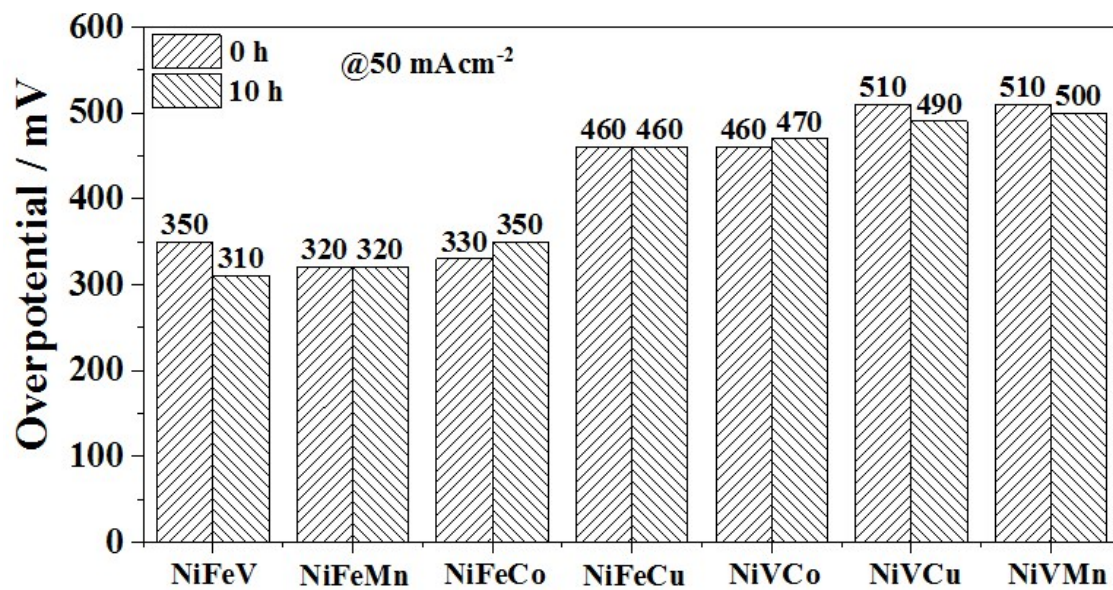


**Figure S12.** The overpotential at a current density of  $50 \text{ mA cm}^{-2}$  for NiFeMn, NiFeCo, NiFeCu, NiVCo, NiVCu, and NiVMn before and after activation for 10 h.

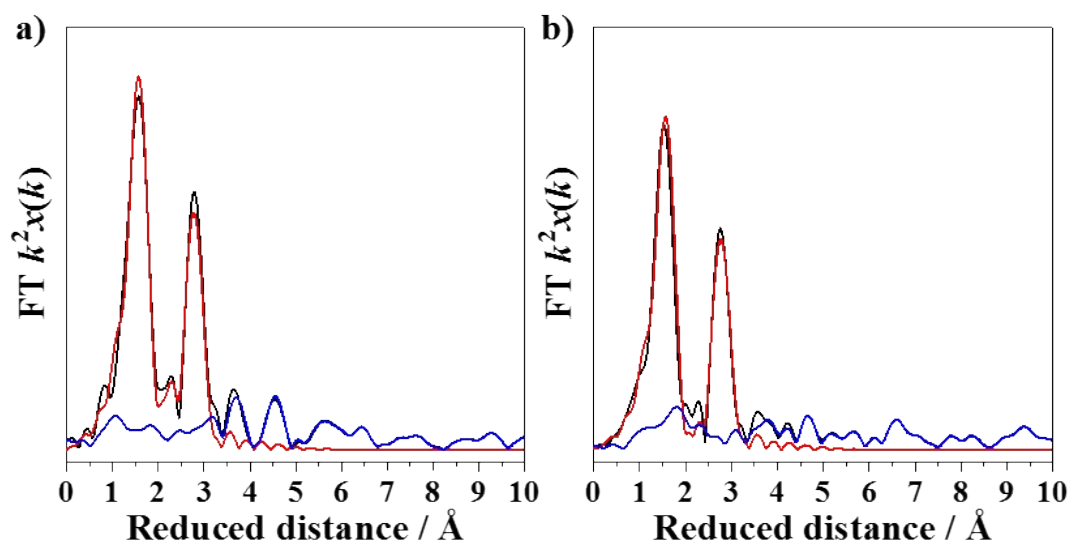


**Figure S13.** FT-EXAFS spectra and fits of Fe K-edges from O-NiFeV-LDH (a), and A-NiFeV-LDH (b). The red and blue lines represent the fitting values. Co K edge XANES spectra.

**Table S1.** Summary of the fitting parameters of Fe K-edge EXAFS curves for the NiFeV-LDH and A-NiFeV-LDH.

Sample	Fe-O		Fe-Fe		D. W.	$\Delta E_0$ (eV)
	R (Å)	CN	R (Å)	CN		
O-NiFeV-LDH	$2.01 \pm 0.007$	$6.8 \pm 0.3$	$2.60 \pm 0.03$	$0.9 \pm 0.3$	0.006 (O)	$-0.7 \pm 0.7$
			$3.24 \pm 0.01$	$4.7 \pm 0.5$		
A-NiFeV-LDH	$2.002 \pm 0.007$	$6.1 \pm 0.2$	$2.58 \pm 0.04$	$0.5 \pm 0.2$	0.008 (Fe)	$4.0 \pm 1.3$
			$3.23 \pm 0.01$	$4.2 \pm 0.4$		

Fe K edge (7112 eV)

Amp:  $0.73 \pm 0.07$  (Fe foil)